





A Bio-inspired Quasi-resonant Compliant Backbone for Low Power Consumption Quadrupedal Locomotion

Edgar A. Parra Ricaurte¹^a, Julian D. Colorado²^b, S. Dominguez¹^c and C. Rossi¹^d

¹Centre for Automation and Robotics UPM-CSIC, Madrid, Spain

²Department of Electronics Engineering, Pontificia Universidad Javeriana, Bogotá, Colombia

Keywords: Bio-inspiration, Quadrupedal Locomotion, Compliant Structures, Power Efficiency.

Abstract: Many quadrupeds are capable of highly power efficient gaits thanks to their flexible backbone. This is used during different stages of the gait in order to store and release elastic energy, also helping a smooth deceleration and a fast acceleration of the different parts of the body involved during running. In this work we present our current studies aimed to reproduce such phenomena for efficient robot locomotion. In addition, we studied how to amplify such effect when the frequency of the oscillations is brought close to the natural resonant frequency of the compliant structure. We demonstrated that a flexible artificial structure representing the backbone, muscle and tendons, driven to quasi-resonant oscillations is capable of dramatically reducing the power required to maintain oscillations. At the same time, these reach a bigger amplitude. Such effect will be used to design fast running and energy efficient quadruped robots.

1 INTRODUCTION


Legged locomotion is of great interest in field robotics because it allows great stability on rough terrains and agile movements, as demonstrated by the latest advances in quadruped robots such as Spot by Boston Dynamics¹. The body of literature in this field is fairly big, focussing mainly in mechatronic design and control. (Raibert, 1986) is one the earliest works dealing with dynamic legged robots, and other walking robots are described in (De Santos et al., 2007), (Semini et al., 2011).


Further works aimed at developing legged robots that not only walk, but that are also capable of galloping at high speeds, such as the BigDog (Raibert et al., 2008), KOLT (Nichol et al., 2004), Scout II (Poulakakis et al., 2005), Star1ETH (Gehring et al., 2013) and the MIT Cheetah 2 (Park et al., 2014). All these robots are capable of robust locomotion on may different terrains. However, the structure of their bodies is rigid. Compared to their natural counterparts, like e.g. cheetahs, horses and greyhounds such feature


does not allow them to take advantage of the flexibility of the trunk in order to be able to gallop at high speed with great power efficiently (Alexander, 1988).


In our current work, we aim at designing a legged robot with high power efficiency and fast speed, therefore we focus precisely on such key feature.

In this topic, several investigations have focused on understanding and developing the bending of the trunk, evidencing three types of flexible trunks: actuated, semi-actuated and passive. In (Culha and Saranlı, 2011) it is shown how galloping performance of a quadrupedal can be improved by placing an actuated joint for flexion and extension of the trunk, and compared this one with a rigid robot body, likewise (Bhattacharya et al., 2019) shows the advantages of actuated spine by means of robot Stoch2. They demonstrated that the former allows increased speed and long stride. In (Eckert et al., 2015) a comparison between 3 types of trunks using the Lynx-robot, one actuated for flexion and extension movements, and two actuated only for the flexion movement, and using a glass fibre rod with different stiffness as passive actuator for extension. In (Phan et al., 2017) the difference between rigid and passive articulated trunk, is investigated, showing that the latter has the advantage of performing longer strides and affects significantly the dynamics of the robot and its power efficiency. In

^a <https://orcid.org/0000-0001-6595-5420>

^b <https://orcid.org/0000-0002-6925-0126>

^c <https://orcid.org/0000-0002-9498-5407>

^d <https://orcid.org/0000-0002-8740-2453>

¹<https://www.bostondynamics.com>

(Tsujiata and Miki, 2011), the stability of gait patterns with variable trunk stiffness is investigated.

It is important to highlight that while in most rigid-bodied quadrupedal robots the legs' mass is considered negligible for the purpose of studying robot's body dynamics, when it comes to flexible backbone legged robots, this plays a key role, since the moving masses of the legs (plus tail and head) and their contact with the ground concur to toe trunk bending that accumulates and releases energy, especially during trot and gallop (Alexander, 1984; Day and Jayne, 2007)².

In this paper we aim at studying and characterising these phenomena, with the additional purpose of demonstrating that a dramatic power saving is obtained driving the oscillations of the trunk to a quasi-resonant regime. Such effect has been studied e.g. in (Maheshwari et al., 2012), (Iida et al., 2012) and (Reis and Iida, 2014) for hopping robots and robots with compliant legs. Such effect has also been demonstrated on flexible backbones for fish-like robots (Coral et al., 2015).

The paper is organised as follows. Section 2 explains the mathematical analysis performed to know the fundamental frequencies and vibration modes for known dimensions of an Aluminum beam. In Section 3 we explain the mechanical design and hardware components of the testbed used for experimental analysis. Section 4 details the control scheme used in order to achieve continuous vibration while maintaining a given frequency. Section 5 reports the results of the experiments, and Section 6 concludes the paper with a discussion on the results and future work.

2 MATHEMATICAL ANALYSIS

For the purpose of concept proving our approach, the trunk of a quadrupedal is modelled as a flexible beam made of aluminum, with two masses at its ends representing the hind and forelegs. The oscillating movement is provided by a mechanical system representing the trunk musculature. The details of the models are shown in Figure 1.

In order to calculate the natural frequencies and mode shapes of a cantilever Euler-Bernoulli beam carrying a point mass, we used the Superposition Method (Rao, 2011), how can be seen in the Figure (2). Using this method, the modal coordinate and

²A similar effect is also present in insects and birds, whose thorax contain compliant structures that accumulate and release energy during the flapping cycle at the benefit of power consumption, but also flight stability, see, e.g. (Zhang and Rossi, 2017; Zhang and Rossi, 2019).

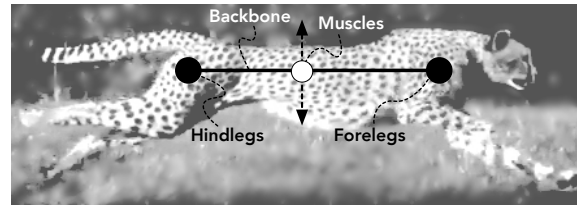


Figure 1: Model of the system.

mode shapes functions must be calculated. These have been calculated by means of separation of variables and Laplace transformation (Skoblar et al., 2017). The model of the cantilever Euler-Bernoulli beam carrying a point mass is defined by the following equation:

$$EI \frac{\partial^4 w}{\partial x^4} + \rho A \frac{\partial^2 w}{\partial t^2} + M \frac{\partial^2 w}{\partial t^2} \delta(x - x_M) = 0 \quad (1)$$

where E the Young's model, I second moment of area, w cross displacement, ρ beam material density, A the cross-section area, M the mass point values and x_M the coordinate of the point mass.

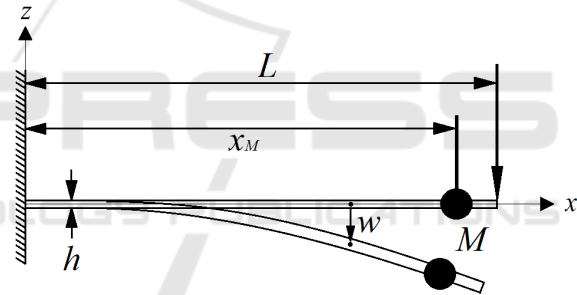


Figure 2: Diagram of Euler-Bernoulli cantilever beam carrying a point mass M .

Taking into account the physical restrictions and the fourth-order partial differential equation (1), it is necessary to have boundary conditions to determine a solution of system. We have four boundary conditions for a cantilever beam, since the number of boundary conditions must coincide with the order of the partial differential equation, which are for clamped-free and free-free conditions. In our case, the former applies.

2.1 Natural Frequencies and Mode Shapes of Clamped-free Boundary Condition

Considering equation (1), the following boundary conditions are needed to find the natural frequencies and mode shapes.

$$w(0,t) = w'(0,t) = w''(L,t) = w'''(L,t) = 0 \quad (2)$$

where w is the lateral displacement of the beam and the derivatives with respect to x are the different conditions of the ends beam. As mentioned before, differential equation (1) is solved by means of separation of variables. Therefore, displacement is defined as the product of two separate functions, which depend one on the position and the other on time.

$$w(x, t) = \psi(x)\sin(\omega t) \quad (3)$$

where $\psi(x)$ is the mode shape and $\sin(\omega t)$ represents of harmonic vibration with angular natural frequency ω . Hence, taking into account the separation of variables, including equation (3) into (1), performing the corresponding derivatives and dividing by $\sin(\omega t)$, we obtain:

$$EI\psi(x)^{(4)} - \rho A\omega^2\psi(x) - M\omega^2\psi(x)\delta(x - x_M) = 0 \quad (4)$$

$$EI\psi(x)^{(4)} - \underbrace{(\rho A + M\delta(x - x_M))}_{\varepsilon(x)}\omega^2\psi(x) = 0 \quad (5)$$

Function $\varepsilon(x)$ called *weighting function*.

Applying the Laplace transform in equation (5) with respect to x coordinate, we obtain:

$$EI[s^4\mathcal{L}\{\psi(x)\} - s^3\psi(0) - s^2\psi(0)' - s\psi(0)'' - \psi(0)'''] - \rho A\omega^2\mathcal{L}\{\psi(x)\} - M\omega^2 e^{-sx_M}\psi(x_M) = 0 \quad (6)$$

Boundary conditions indicated in (2) must be maintained despite applying the separation of variable (3). Since as aforementioned above, this conditions helps to determine a solution taking into account the physical restrictions and the order of the partial differential equation. Therefore, it being possible to obtain the following conditions with the mode shape:

$$\psi(0) = \psi(0)' = \psi(L)'' = \psi(L)''' = 0 \quad (7)$$

Applying these conditions to equation (6), the following expression is obtained:

$$s\psi(0)'' + \psi(0)''' + \frac{M\omega^2}{EI}e^{-sx_M}\psi(x_M) = \mathcal{L}\{\psi(x)\} \left(s^4 - \frac{\rho A\omega^2}{EI} \right) \quad (8)$$

By rearranging equation (8), we obtain:

$$\mathcal{L}\{\psi(x)\} = \psi(0)'' \frac{s}{s^4 - k^4} + \psi(0)''' \frac{1}{s^4 - k^4} + \frac{M\omega^2\psi(x_M)}{EI} \frac{e^{-sx_M}}{s^4 - k^4} \quad (9)$$

where k is the *wave number*, which can be calculated with the following expression:

$$k = \left(\frac{\omega^2 \rho A}{EI} \right)^{1/4} \quad (10)$$

Performing the inverse transform, the following expression is obtained:

$$\psi(x) = \psi(0)'' \frac{\cosh(kx) - \cos(kx)}{2k^2} + \psi(0)''' \frac{\sinh(kx) - \sin(kx)}{2k^3} + \frac{M\omega^2\psi(x_M)}{EI} U(x - x_M) \frac{\sinh(kx - kx_M) - \sin(kx - kx_M)}{2k^3} \quad (11)$$

To calculate the values of $\psi(0)''$ and $\psi(0)'''$, the function (11) is derived taking into account the conditions $\psi(L)'' = \psi(L)''' = 0$. Therefore, the second and third derivative of the function is performed and change x by L . Obtaining the following expressions:

$$0 = \psi(L)'' = \psi(0)'' \overbrace{(\cosh(kL) + \cos(kL))}^A + \frac{\psi(0)'''}{k} \overbrace{(\sinh(kL) + \sin(kL))}^B + \frac{M\omega^2\psi(x_M)}{EI k} \quad (12)$$

$$0 = \psi(L)''' = \psi(0)'' k \overbrace{(\sinh(kL) - \sin(kL))}^C + \psi(0)''' \overbrace{(\cos(kL) - \cosh(kL))}^D + \frac{M\omega^2\psi(x_M)}{EI} \overbrace{(\cosh(kL - kx_M) + \cos(kL - kx_M))}^G \quad (13)$$

The expressions indicated by letters A, B, C, D, F and G, in (12) and (13) are used for convenience in order to compute the values $\psi(0)''$ and $\psi(0)'''$. Then,

$$0 = \psi(0)'' A + \frac{\psi(0)'''}{k} B + \frac{M\omega^2\psi(x_M)}{EI k} C \quad (14)$$

$$0 = \psi(0)'' k D + \psi(0)''' F + \frac{M\omega^2\psi(x_M)}{EI} G \quad (15)$$

and

$$\psi(0)'' = \frac{M\omega^2\psi(x_M)}{EI k} \overbrace{\left[\frac{BG - CF}{BD - AF} \right]}^R \quad (16)$$

$$\psi(0)''' = \frac{M\omega^2\psi(x_M)}{EI} \overbrace{\left[\frac{AG - CF}{BD - AF} \right]}^S \quad (17)$$

Including (16) and (17) into (11), and rearranging the expression the mode shape is obtained:

$$\psi(x) = \frac{M\omega^2\psi(x_M)}{2EI k^3} [R(\cosh(kx) - \cos(kx)) - S(\sinh(kx) - \sin(kx)) + U(x - x_M)(\sinh(kx - kx_M) - \sin(kx - kx_M))] \quad (18)$$

By obtaining the mode shape, the natural frequencies of the clamped-free model can be calculated.

For this research was used a aluminium beam with height $h = 0.015$ m, width $w = 0.00302$ m and length $L = 0.732$ m, density $\rho = 2700$ kg/m³ and Young's module $E = 70$ GPa. It was used a sphere mass of ABS plastic with a mass $M = 0.0464$ kg, being this mass positioned at $x_M = 0.710$ m.

With the previous data and changing x by x_M in equation (18) it is obtained an expression in the form $f(k) = 0$, which allows to find the values of k , wave number. And from equation (10), the natural frequencies can be obtained, confirming the accuracy of the analytical data with Abaqus 2019 was used. Table 1 shows the four main frequencies computed for the beam.

Table 1: Natural frequencies of the clamped-free boundary conditions.

Natural Frequencies No	Abaqus Data Hz	Analytic Data Hz	Analytic Data rad/s
1	2.704	2.704	16.993
2	23.423	23.424	147.182
3	71.947	71.961	452.145
4	147.710	147.769	928.463

3 TEST PLATFORM

In order to experimentally assess the result of the mathematical analysis described in the previous section, a platform was created that could produce continuous oscillations.

3.1 Mechanical Design

Figure 3 depicts the main elements of the system, composed of (1) a metallic axis of aluminium on which (2) two ABS plastic 3D printed covers are fastened, both holding (3) two aluminum rails. On these rails (4) two sliding bases, which with the help of 4 bearings allow vertical movement of this bases.

These sliding bases together with the (5) pinion-motor form a rack-pinion system that convert the circular movement to a lineal-vertical movement. (6) A platform, that is fastened in the sliding bases, holds in the middle the (8) aluminum beam. To maintain fixed the pinion-motor system on the metallic axis of aluminium, this one is held with (7) a ABS plastic 3D printed base. Finally, (9) two ABS plastic 3D printed masses are held on the aluminum beam.

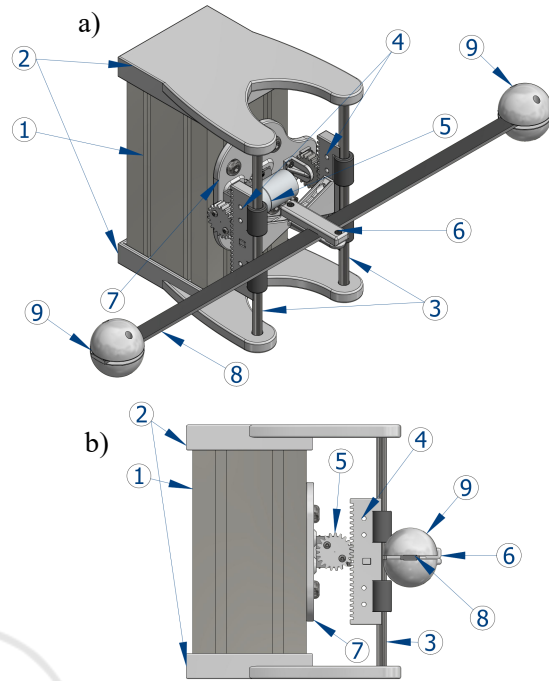


Figure 3: a) Isometric and b) lateral view of the mechanism with scale beam.

The following list specifies each of the components indicated in Figure 3.

1. Metallic axis: Extruded aluminum profile being 181 mm of height, 90 mm in width and 90 mm in depth. It has 8 rail spaces where pieces with screw of M8 can be held.
2. ABS plastic 3D printed covers: They are two ABS plastic 3D printed covers being 20 mm in height, 100 mm in width, 170 mm in depth and filling of 70%.
3. Aluminum rails: They are two aluminum rails with diameter of 8 mm and 191 mm in length.
4. Sliding bases: They are two ABS plastic 3D printed sliding bases being 100 mm in height, 10 mm in width and 25 mm in deep. They have got a lineal rack-teeth with module of 1.3 mm.
5. Pinion-motor: The system is composed by a 12V brushed DC motor with a 34:1 metal spur gear-box with its corresponding 48 CPR encoder and an ABS plastic 3D printed pinion with a width of 8 mm, module of 1.3 mm and radius 15 mm with a filling of 70%.
6. Platform: It is ABS plastic 3D printed platform being 30.23 mm in height, 87.1 mm in width and 63.5 mm in depth. Its design allows to hold the aluminium beam by mean of M3 Allen bolts.

7. Base: It is ABS plastic 3D printed base being 108 mm in height, 111.25 in width and 8 mm in depth. Its design allows to hold the pinion-motor by means of M3 Allen bolts and fixed to the metal axis by means of M8 Allen bolts.
8. Aluminum beam: Aluminum rectangular beam being 1464 mm long, 1.5 mm in height and 3.02 mm in width.
9. Plastic masses: Four semi-spheres of ABS plastic 3D printed masses. Its design allows 2 semi-spheres to be fastened by means of Allen M3 bolts, being the flat part of the semi-spheres, which in turn, by pressure are attached to each end of the aluminum beam, having two masses at each end of the beam.

3.2 Electronics

The scheme shown in Figure 4 illustrates the different devices in the hardware components. The system uses the Power Supply of 12V and 5A that powered a medium-power 12V brushed DC Motor by means of 9 Amp Pololu High-Power Motor Driver. It can also be seen a Raspberry Pi 3 Quad Core BCM2837 ARMv8 1.4 GHz single-Board computer running Ubuntu Linux 16.04 and Robotic-Operating System (ROS) Kinetic middleware, it takes the 48 CPR Encoder signals and commands the DC Motor rotation. It also has an Arduino Mega ATmega2560 16 MHz which takes the analog signals of SparkFun Hall-Effect Current Sensor Breakout ACS712 and Analog Circuit that improves the flex sensors analog signal by reducing noise, being the latter, 4 Brewer Science Inflex Flex Sensors. The High-Power Motor Driver, Current Sensor and Analog Circuit are powered with 5V by the Power Supply for proper operation.

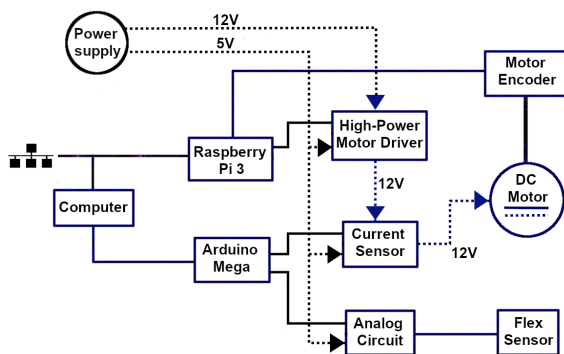


Figure 4: Schematic electronic setup.

The flex sensor varies its resistance when it is bent. Figure 5 depicts the voltage divider circuit imple-

mented, which consists of the flex sensor, a LM324N operational amplifier and a 10KΩ resistor.

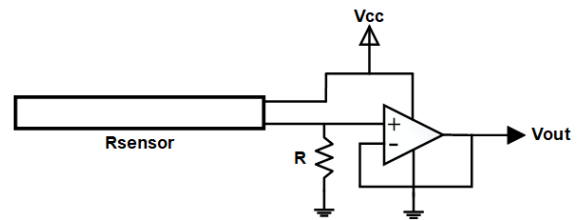


Figure 5: Schematic sensor connection.

In order to filter out the noise of the sensors, and improve the quality of the sensors signals, 4 flex sensors have been mounted near the center of the bar, since from that point the aluminium beam is held by the platform and a better measure of flexion can be obtained, as shown in Figure 6.

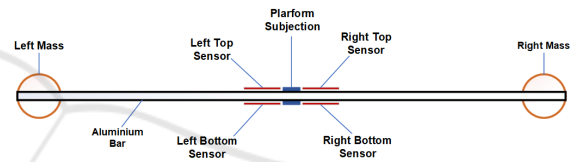


Figure 6: Scheme position of the platform subsection, sensors and masses in the aluminium bar.

The signals of each couple of sensors are combined performing an analog addition and subtraction operation with operational amplifiers. Figure 7 depicts the circuit used. It consists of a LM324N operational amplifier, five 10KΩ resistors and a potentiometer, the latter being the one that generates and offset that helps moving the signal in the appropriate voltage limits.

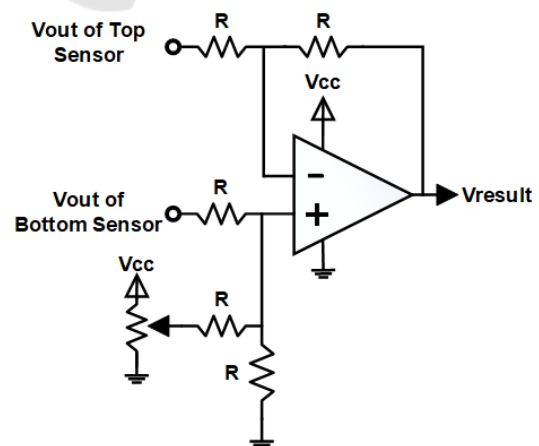


Figure 7: Scheme of the adder-subtractor circuit.

4 CONTROL OF THE SYSTEM

For the control of the system, we implemented a phase advance control. Therefore, to identify the system, the transient response to a step input was determined. The step input was 3.283V to the High-Power Motor Driver, that drives the DC Motor. The motor encoder signals output were taken and the angular velocity, between 23 and 21.56 rad/s, was obtained as shown in Figure 8.

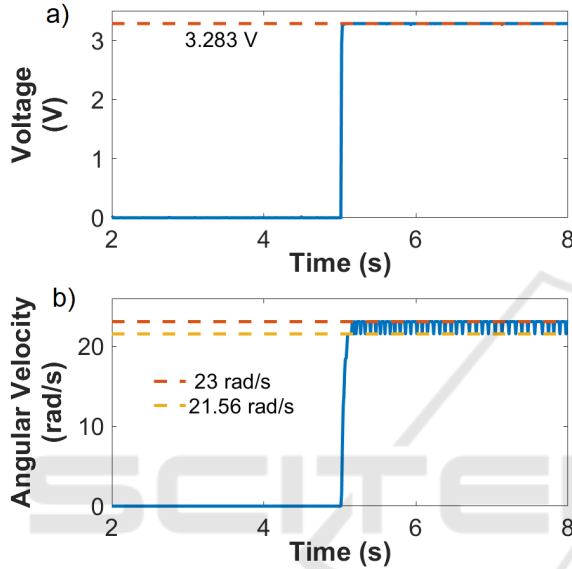


Figure 8: a) Input step and b) the response of the system.

Using the System Identification Toolbox of the Matlab[®] 2019a, the transfer function of the system was identified:

$$G(s) = \frac{254.1}{s + 36.37} \quad (19)$$

As depicted in Figure 9, the response of the system is critically damped. To carry out the phase advance control, it was decided to use the root locus method setting the parameters to make the system underdamped. For the purpose of system identification, a step input signal was used.

A rate damping of 0.8 and a natural undamped frequency of 35 rad/s has been set experimentally, obtaining the following transfer function for the control:

$$R(s) = 6 \left[\frac{s + 29.0047}{s + 42.2345} \right] \quad (20)$$

For the implementation of the control, Simulink of Matlab[®] 2019a was used, having ROS as a middleware for the communication between Simulink and the system hardware.

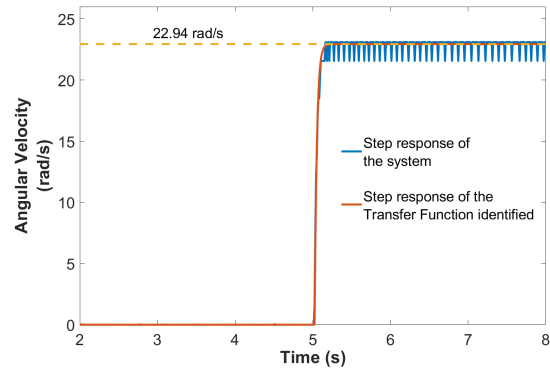


Figure 9: Step response of the system and the Transfer Function identified.

5 EXPERIMENTAL RESULTS

To demonstrate low power consumption that can be achieved using a flexible backbone when it is driven to a quasi-resonant frequency, we measured the power consumption which is needed to keep the flexible beam oscillating at different frequencies of the sinusoidal input signal ranging from 13 to 20 rad/s with 1 rad/s steps (recall that the theoretical quasi-resonant frequency computed is 17 rad/s as is depicted in figure 10).

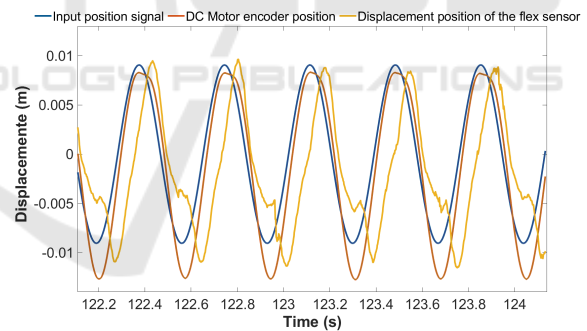


Figure 10: Comparison graph of the Input position signal, DC Motor encoder position and displacement position of the flex sensor during 3 seconds for a frequency of 17rad/s.

It is important for this investigation to verify that the mobile platform (component (6) in Figure 3) that holds the aluminium beam, follows the sinusoidal input signals with their respective frequency. For this reason a frequency analysis of the DC Motor encoder signal and flex sensors signal were performed. As can be seen in Figure 11, the DC Motor encoder signals, that measure the rotation position of the DC Motor, followed the eight sinusoidal test input signals with a error under 12%. Also, the frequency analysis of the flex sensors that measure the flexion of aluminium beam carrying a point mass, followed the eight sinu-

soidal test input signals with a error less than 10%. Such errors of the frequency analysis of the DC Motor encoder and the flex sensors signals are admissible for our purposes.

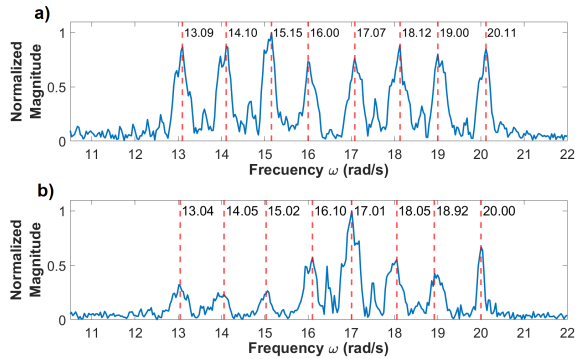


Figure 11: Frequency analysis of a) the DC Motor encoder signal and b) the flex sensors signal of the Aluminum beam.

For the purpose of experimental assessment, the current consumption, voltage and the displacement of the flex sensor were recorded for 10 seconds for each of the eight frequencies. We calculated the *root mean square (rms)* values of the current consumption and the voltage for this each period of time to compute the power consumed.

As can be seen in Figure 12, for the first frequency values, low power consumption and low displacement were obtained. As the frequency value increased, power consumption increased until the quasi-resonant frequency was reached (at approximately 17rad/s), where a dramatic decrease in power consumption and an increase in displacement can be observed. Subsequently, when the frequency increases, leaving the quasi-resonant frequency, an increase in power consumption and a decrease in displacement can be observed.

6 CONCLUSIONS

The purpose of this work was to demonstrate how a flexible backbone for a quadruped robot can greatly help the to achieve a low power consumption of the gait when its oscillations are brought close to resonance. Considering the theory of resonance in flexible materials, and using a simplified model consisting of an aluminium beam with two masses at its two ends, we could verify that driving it to a controlled quasi-resonance frequency, the power needed for maintaining its oscillations is dramatically reduced.

This is a first step to develop fast-running and power efficient quadruped robots with a bio-inspired

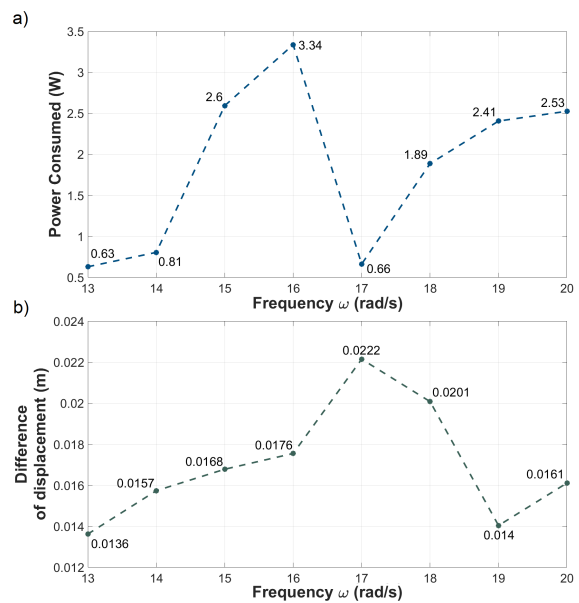


Figure 12: a) The power consumed and b) the difference of displacement versus frequency.

trunk. Experimental results confirmed our working hypothesis.

Future work will be focused on improving the control systems, e.g. using hysteresis control (Ogata, 1997), where the amplitude and activation times are controlled, being our expectations that will further reduce power consumption.

Another important line of research is designing a mechatronic system to actively change the stiffness of the spine in a controlled way. In fact, different stiffness would make the trunk resonate at different frequencies, i.e. different gait speeds. Therefore, it would be possible to have different power efficient gaits at different paces (and hence running speed).

This is indeed feasible. Different strategies can be devised in order to change the stiffness of a material (see, e.g., (Wang et al., 2018), where four methods that can be used to change the stiffness material are mentioned: *thermal*, *pressure*, *magnetic field* and *electric field induced*), including mechanical arrangements, as well as the use of *functional* materials.

In conclusion, we believe that semi-active compliant structures are a promising research field for future robotic systems. This paper is our first step in this direction.

ACKNOWLEDGEMENTS

This research has received funding from the European Union’s Horizon 2020 research and innova-

tion program under grant agreement No. 820971Ê (“ROBOMINERS”) and from the RoboCity2030-DIH-CM, Madrid Robotics Digital Innovation Hub, S2018/NMT-4331, funded by Programas de Actividades I+D en la Comunidad de Madrid and co-funded by Structural Funds of the EU. The authors acknowledge the help of Prof. Maria Consuelo Huerta of the Department of Structural Mechanics and Industrial Constructions and PhD. Álvaro Nieto Carrero of the Mechanical Engineering Department of the Universidad Politécnica de Madrid.

REFERENCES

- Alexander, R. M. (1984). Elastic energy stores in running vertebrates. *American Zoologist*, 24(1):85–94.
- Alexander, R. M. (1988). Why mammals gallop. *American zoologist*, 28(1):237–245.
- Bhattacharya, S., Singla, A., Dholakiya, D., Bhatnagar, S., Amrutur, B., Ghosal, A., Kolathaya, S., et al. (2019). Learning active spine behaviors for dynamic and efficient locomotion in quadruped robots. In *2019 28th IEEE International Conference on Robot and Human Interactive Communication (RO-MAN)*, pages 1–6. IEEE.
- Coral, W., Rossi, C., and Curet, O. (2015). Free vibration analysis of a robotic fish based on a continuous and non-uniform flexible backbone with distributed masses. *The European Physical Journal Special Topics*, 224(17):3379–3392.
- Culha, U. and Saranlı, U. (2011). Quadrupedal bounding with an actuated spinal joint. In *2011 IEEE International Conference on Robotics and Automation*, pages 1392–1397. IEEE.
- Day, L. M. and Jayne, B. C. (2007). Interspecific scaling of the morphology and posture of the limbs during the locomotion of cats (felidae). *Journal of Experimental Biology*, 210(4):642–654.
- De Santos, P. G., Garcia, E., and Estremera, J. (2007). *Quadrupedal locomotion: an introduction to the control of four-legged robots*. Springer Science & Business Media.
- Eckert, P., Spröwitz, A., Witte, H., and Ijspeert, A. J. (2015). Comparing the effect of different spine and leg designs for a small bounding quadruped robot. In *2015 IEEE International Conference on Robotics and Automation (ICRA)*, pages 3128–3133. IEEE.
- Gehring, C., Coros, S., Hutter, M., Bloesch, M., Hoepflinger, M. A., and Siegwart, R. (2013). Control of dynamic gaits for a quadrupedal robot. In *2013 IEEE international conference on Robotics and automation*, pages 3287–3292. IEEE.
- Iida, F., Reis, M., Maheshwari, N., Yu, X., and Jafari, A. (2012). Toward efficient, fast, and versatile running robots based on free vibration.
- Maheshwari, N., Yu, X., Reis, M., and Iida, F. (2012). Resonance based multi-gaited robot locomotion. In *2012 IEEE/RSJ International Conference on Intelligent Robots and Systems*, pages 169–174.
- Nichol, J. G., Singh, S. P., Waldron, K. J., Palmer Iii, L. R., and Orin, D. E. (2004). System design of a quadrupedal galloping machine. *The International Journal of Robotics Research*, 23(10-11):1013–1027.
- Ogata, K. (1997). *Modern control systems*. Prentice Hall.
- Park, H.-W., Chuah, M. Y., and Kim, S. (2014). Quadruped bounding control with variable duty cycle via vertical impulse scaling. In *2014 IEEE/RSJ International Conference on Intelligent Robots and Systems*, pages 3245–3252. IEEE.
- Phan, L. T., Lee, Y. H., Lee, Y. H., Lee, H., Kang, H., and Choi, H. R. (2017). Study on quadruped bounding with a passive compliant spine. In *2017 IEEE/RSJ International Conference on Intelligent Robots and Systems (IROS)*, pages 2409–2414. IEEE.
- Poulakakis, I., Smith, J. A., and Buehler, M. (2005). Modeling and experiments of untethered quadrupedal running with a bounding gait: The scout ii robot. *The International Journal of Robotics Research*, 24(4):239–256.
- Raibert, M., Blankespoor, K., Nelson, G., and Playter, R. (2008). Bigdog, the rough-terrain quadruped robot. *IFAC Proceedings Volumes*, 41(2):10822–10825.
- Raibert, M. H. (1986). *Legged robots that balance*. MIT press.
- Rao, S. S. (2011). *Mechanical vibrations*. Pearson Higher 5th Ed.
- Reis, M. and Iida, F. (2014). An energy-efficient hopping robot based on free vibration of a curved beam. *IEEE/ASME Transactions on Mechatronics*, 19(1):300–311.
- Semini, C., Tsagarakis, N. G., Guglielmino, E., Focchi, M., Cannella, F., and Caldwell, D. G. (2011). Design of hyq—a hydraulically and electrically actuated quadruped robot. *Proceedings of the Institution of Mechanical Engineers, Part I: Journal of Systems and Control Engineering*, 225(6):831–849.
- Skoblar, A., Žigulić, R., Braut, S., and Blažević, S. (2017). Dynamic response to harmonic transverse excitation of cantilever euler-bernoulli beam carrying a point mass. *FME Transactions*, 45(3):367–373.
- Tsujita, K. and Miki, K. (2011). A study on trunk stiffness and gait stability in quadrupedal locomotion using musculoskeletal robot. In *2011 15th International Conference on Advanced Robotics (ICAR)*, pages 316–321. IEEE.
- Wang, L., Yang, Y., Chen, Y., Majidi, C., Iida, F., Askounis, E., and Pei, Q. (2018). Controllable and reversible tuning of material rigidity for robot applications. *Materials Today*, 21(5):563–576.
- Zhang, C. and Rossi, C. (2017). A review of compliant transmission mechanisms for bio-inspired flapping-wing micro air vehicles. *Bioinspir. Biomim.*, 12(2).
- Zhang, C. and Rossi, C. (2019). Effects of elastic hinges on input torque requirements for a motorized indirect-driven flapping-wing compliant transmission mechanism. *IEEE Access*, 7:10368–13077.